

CONFIDENTIAL

5
Copy
RM L55L19a

52

NACA RM L55L19a

UNCLASSIFIED



RESEARCH MEMORANDUM

FOR REFERENCE

NOT TO BE TAKEN FROM THIS ROOM

FLOW FIELD EFFECTS ON STATIC STABILITY AND CONTROL
AT HIGH SUPERSONIC MACH NUMBERS

By Edward F. Ulmann and Herbert W. Ridyard

Langley Aeronautical Laboratory
Langley Field, Va.

CLASSIFICATION CHANGED

UNCLASSIFIED

To

NATIONAL ADVISORY COMMITTEE
FOR AERONAUTICS

WASHINGTON

March 8, 1956

This material contains information affecting the National Defense of the United States within the meaning of the espionage laws, Title 18, U.S.C., Secs. 793 and 794, the transmission or revelation of which in any manner to an unauthorized person is prohibited by law.

CLASSIFIED DOCUMENT

CONFIDENTIAL

*Authority of JPA # 55
Date 8-1-64
gu*



NATIONAL ADVISORY COMMITTEE FOR AERONAUTICS

RESEARCH MEMORANDUM

FLOW-FIELD EFFECTS ON STATIC STABILITY AND CONTROL

AT HIGH SUPERSONIC MACH NUMBERS

By Edward F. Ulmann and Herbert W. Ridyard

SUMMARY

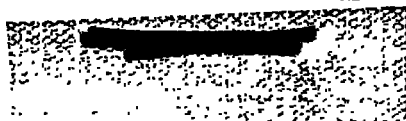
Recent wind-tunnel investigations of aircraft-type configurations at Mach numbers 4.06 and 6.86 have provided data which show that flow-field interference is of primary importance in stability and control calculations at high supersonic Mach numbers and that the location of stabilizing and control surfaces that give highest effectiveness can be determined by theoretical studies of these flow fields. A method has been derived which predicts the trend of downwash around a circular body as the angle of attack is increased. A method has also been derived which gives good predictions of the tail contributions to lateral stability through a considerable angle-of-attack range.

INTRODUCTION

The importance of flow-field interference at supersonic Mach numbers below 3.0 has been discussed in reference 1. These effects become increasingly important as the Mach number is increased beyond 3.0. In this paper, some illustrations of the effects of these flow fields will be presented and it will be shown that, for close coupled configurations, it is possible to predict some effects of flow-field interference on longitudinal and lateral stability and control.

Figures 1 and 2 present schlieren photographs of the flow around a model that has been extensively tested at Mach numbers 4.06 and 6.86 in the Langley 11-inch hypersonic tunnel and the Langley 9- by 9-inch Mach number 4 blowdown jet (refs. 2 to 8). The model has a tapered wing and a cruciform tail arrangement. Several important features of the flow around this model can be seen in these photographs. The fuselage is fairly blunt and the resultant strong bow wave causes total-pressure losses that reduce the lift of the wing and the tail.

In the side view (fig. 2) the wing is obscured by the body but the shocks from the wing can be seen. These shocks enclose regions of greatly different dynamic pressure and Mach number above and below the wing. The vertical tails are almost completely covered by these regions at both Mach numbers but, as will be shown, this is not necessarily a bad situation



if the tail surfaces are arranged properly. It is obvious from the photographs and from considerations of shock-field strength that these flow fields are nonisentropic and that their effects on the tail surfaces cannot be accurately predicted by potential-theory or linear-theory methods.

It should be noted that this paper will not consider the vortex type of interference. At high supersonic Mach numbers, the wing trailing vortices would not be expected to have much effect on the tail surfaces for close coupled configurations such as that shown in figure 1, which have a wing span considerably larger than the tail span. This supposition is supported by experimental data which gave a tail efficiency (ratio of the lift-curve slope of the tail in the presence of the body to the lift-curve slope of the tail in the presence of the body-wing configuration) of 94 percent at zero angle of attack and Mach number 6.86 for the trapezoidal wing model shown in figure 1.

SYMBOLS

C_L	lift coefficient, $\frac{\text{Lift}}{q_\infty S}$
C_Y	lateral-force coefficient, $\frac{\text{Lateral force}}{q_\infty S}$
C_m	pitching-moment coefficient about center of gravity, $\frac{\text{Pitching moment}}{q_\infty S \bar{c}}$
C_n	yawing-moment coefficient about center of gravity, $\frac{\text{Yawing moment}}{q_\infty S b}$
C_{Y_β}	rate of change of lateral-force coefficient with angle of sideslip
C_{n_β}	rate of change of yawing-moment coefficient with angle of sideslip
ΔC_{Y_β}	increment in C_{Y_β} due to the addition of one or more vertical tail surfaces to a configuration
ΔC_{n_β}	increment in C_{n_β} due to the addition of one or more vertical tail surfaces to a configuration

α	angle of attack, deg
β	angle of sideslip, deg
b	wing span
\bar{c}	wing mean geometric chord
ϵ	effective downwash angle of the horizontal tail, deg
i_t	horizontal-tail incidence angle, deg
M	Mach number
q	dynamic pressure
R	Reynolds number based on \bar{c}
S	total wing area
Subscripts:	
∞	free-stream value
U	in shock field from upper surface of a wing
L	in shock field from lower surface of a wing

LONGITUDINAL STABILITY AND CONTROL

Some effects of these flow fields on the longitudinal stability and control of this model will be considered first. A very important consideration regarding longitudinal stability is, of course, the location of the horizontal tail surfaces. Any analysis to determine the optimum location of the horizontal tail must consider the local dynamic-pressure and Mach number variations in the region of the tail, the downwash velocities, and the effects of the viscous wake.

At high supersonic Mach numbers, the horizontal tail surfaces may be directly affected by the compression and expansion fields from the wing, since these fields are swept back sharply. Thus it is instructive to examine the possible variations of dynamic pressure in the shock fields from a wing through the Mach number range. In figure 3 the ratio of the dynamic pressure in the flow fields influenced by the constant-thickness portion of a 4-percent-thick wedge-slab airfoil at an angle of attack of 15° is presented. From the figure, it is seen that the dynamic pressure

in the compression field from the lower surface increases greatly with Mach number, whereas the dynamic pressure in the expansion field from the upper surface becomes so low as to be negligible at Mach numbers around 8 and 10. The ratios of the lift coefficients of surfaces in these regions to the lift coefficients of the same surfaces in the free stream would be higher in the compression field and lower in the expansion field than the dynamic-pressure ratios in figure 3. The reason for this is that the lift-curve slopes increase in the compression field because of the lower local Mach number in this region and decrease in the expansion field because of the higher local Mach number. Flow separation from the upper surface of such a wing would become a consideration at some angle of attack depending on the flow conditions. It is of interest to note that separation and the condition of high Mach number and low dynamic pressure which exists above the wing without separation both act to decrease the effectiveness of any aerodynamic surfaces located in this region.

A theoretical example of the effects of these dynamic-pressure variations and the accompanying Mach number and downwash variations on the stability and control effectiveness of horizontal tail surfaces is presented in figure 4. For simplicity of presentation, the two-dimensional flow field around a flat-plate wing is shown at a Mach number of 4.0. A 10° single-wedge horizontal tail surface is placed in three locations: in the expansion field from the upper surface of the wing, in the plane of the wing, and in the compression field from the lower surface of the wing. A surface at location C (in the compression field) will be in the region of high dynamic pressure as was indicated in figure 3, but the downwash angle at location C is equal to the angle of attack of the wing, and $d\epsilon/d\alpha = 1$. Thus, the tail surface will be at zero angle of attack to the local flow and will produce no lift and therefore no stabilizing moment, as is indicated in the table in figure 4.

The same downwash situation will exist at tail location A, and the pitching-moment contribution of a tail surface there is also zero, as indicated in the table. A stabilizer located in the region between the shock and the expansion from the wing trailing edge (as at location B) will be in a region of very small upwash (about 0.4° at this angle of attack and Mach number). The dynamic pressure will be close to the free-stream value; $d\epsilon/d\alpha$ will be very close to zero; and the tail will produce a stabilizing moment. In reference 1, Love has shown that, as wing thickness and leading-edge bluntness are increased, there is a large increase in upwash velocity at wing trailing edges at high angles of attack. However, this upwash decreases rapidly with distance downstream from the trailing edge. The configurations which will be discussed in this paper have thin wings and small leading-edge bluntness and should, therefore, produce only small values of upwash at the tail.

If these surfaces are considered to be all-movable control surfaces, their effectiveness $\partial C_m / \partial i_t$ relative to the in-line tail at location B is indicated in the table as $\left(\frac{\partial C_m}{\partial i_t} \right) / \left(\frac{\partial C_m}{\partial i_t} \right)_B$. (See fig. 4.) The control at location A would be only 0.6 as effective as that at B; a control at location C would be three times as effective as one at B; but the zero stabilizing moment and the obvious difficulties with ground clearance might well preclude the use of the low tail position.

However, a tail location slightly below the wing chord plane should be used to keep the tail out of the wing wake at low angles of attack, since at high Mach numbers and low Reynolds numbers a thick boundary layer is formed on the wing resulting in a thick wake which causes serious losses in tail effectiveness.

Figure 5 presents data obtained on the trapezoidal wing model which show the same variations of stability with tail location indicated by the simplified analysis presented in figure 4. The variation of pitching-moment coefficient with angle of attack is presented at $M = 6.86$ for the trapezoidal wing model (fig. 1) with three tail arrangements: a "plus" tail and high and low tails with 17° dihedral. At the top of figure 5, the locations of these tail surfaces are shown relative to the flow field from the wing root at an angle of attack of 2° . As discussed previously, a configuration having a tail surface located just below the wake should have the highest stability, and this is confirmed by the experimental data - the plus tail configuration being the most stable.

Thus, it has been shown that for this configuration the trends of stability changes with tail location can be predicted from considerations of the two-dimensional wing flow field. But when actual values of the stability and control parameters are required, the body flow field with its upwash, the total-pressure loss caused by the bow wave, and the local dynamic-pressure changes must be considered.

Figure 6 compares experimental effective downwash values for the complete-model and the body-tail configurations with a theoretical prediction of local downwash angle at the root chord of the horizontal stabilizer. It is seen that both the body-tail and the complete-model configurations produce upwash at low angles of attack. These upwash values decrease at moderate angles of attack and change to downwash at high angles of attack.

The theoretical method is based on body crossflow theory and takes into account the large decreases in the total pressure of the crossflow which occur when the crossflow velocity is supersonic. The method was used to estimate the local downwash angles at the body surface and these values, shown as the long-dashed curve in figure 6, indicate the same

trend with angle of attack as the experimental effective downwash angles for the body-tail configuration. The trend is obviously quite different from potential theory which predicts a constantly increasing upwash with angle of attack.

In order to investigate the magnitude of the interference effects for this configuration, the lift and pitching-moment curves for the body-wing, the body-tail, and the body-wing-tail combinations are compared in figures 7 and 8 with the curves obtained by taking the sum of the theoretical lifts and pitching moments of the appropriate components. For most cases the difference between the experimental and the summation theories indicates that there are fairly large interactions in certain angle-of-attack ranges for these configurations.

The effect of tail location on longitudinal control as obtained from tests of the model with high and low horizontal tail surfaces with positive and negative dihedral is shown in figure 9. The change in pitching moment for a tail deflection of -10° is presented, and the lower tail configuration shows much greater effectiveness as angle of attack is increased, since the tail surfaces move into the region of higher local dynamic pressure and lower Mach number produced by the wing as indicated by the simplified analysis (fig. 4).

LATERAL STABILITY

The next part of the paper will be devoted to a discussion of the effects of shock-field interaction on lateral stability derivatives and a method of predicting these effects.

The effect of adding the wing to the body on the variation of the directional stability parameter $C_{n\beta}$ with angle of attack for the test airplane model at Mach number 6.86 is presented in figure 10. The data indicate that at angles of attack greater than 10° the wing produces a stable increment of yawing moment due to the effect of the compression field from the wing lower surface on the afterbody. Data have also been obtained on high and low wing configurations which show a greater increase in $C_{n\beta}$ with angle of attack for the high wing location, as would be expected.

Figure 11 presents the effect of tail arrangement on the variation of the directional stability parameter through the angle-of-attack range. With no vertical tails present there is a considerable increase in stability as the angle of attack is increased.

The upper and lower vertical tails produce about the same increment in directional stability at an angle of attack of 0° , but the contribution of the upper tail decreases as the angle of attack increases, whereas that of the lower tail increases. At an angle of attack of 16° , the lower

tail configuration has the same value of $C_{n\beta}$ as the two-tail configuration, showing that an upper vertical stabilizer may become totally ineffective at high Mach numbers and high angles of attack. The same trends were also found at Mach number 4 in tests of the same model (ref. 7).

A method has been derived to predict these effects of angle of attack on the lateral stability parameters. In this method the sidewash field produced by yawing the body predicted by potential theory is superimposed on the shock-expansion fields from the wing, and the forces and moments on the vertical-tail surfaces are obtained by a strip-theory method. This method has been used to calculate the increments in $C_{n\beta}$ and $C_{y\beta}$ due to the addition of the vertical tail surfaces to the airplane configuration, and a comparison of the theoretical and experimental values of these increments at Mach number 4.06 is presented in figure 12. The computed values of $\Delta C_{y\beta}$ through the angle-of-attack range are in excellent agreement with the experimental values for the three tail arrangements. The predictions of $\Delta C_{n\beta}$ are also good for the configuration with upper and lower vertical tails, but the predictions for the upper tail alone and the lower tail alone are less accurate, although the trend with angle of attack is given correctly for the lower tail configuration. These increments have been obtained with and without horizontal tails on the model, and show very little effect of the horizontal tail surfaces as would be predicted by the theory.

Figure 13 presents the same comparison at Mach number 6.86. The trends are estimated very accurately, but the absolute values of the slope increments are usually too high. It was realized that the predictions were probably too high because the total-pressure losses through the body shock wave had not been considered. In order to check this, the flow field around the body at zero angles of attack and sideslip was calculated by the method of characteristics, and the increments in side force and yawing moment on the vertical stabilizers in this flow field were computed. The results for the configuration with both upper and lower tails are indicated by the short lines on the zero angle-of-attack ordinate and show better agreement with experiment than the results of the method which does not consider the losses through the body bow wave.

Theoretical calculations of $C_{y\beta}$ and $C_{n\beta}$ and their variations with angle of attack have been made by this method for two other configurations at $M = 4.06$. These configurations (fig. 14) have wings and tails with sharp leading edges and wedge slab sections. A comparison of the theoretical and experimental results is presented in figure 15. The agreement was better than that obtained for the trapezoidal wing model, probably because of the sharp leading-edge wing and tail airfoil sections and the rectangular plan form of the wing. The agreement for the model

with delta tail surfaces was about as good as that shown in this figure for the trapezoidal tail surfaces.

CONCLUDING REMARKS

The analysis of the data presented here has shown that flow-field interference is of primary importance in stability and control calculations at high supersonic Mach numbers and that the location of stabilizing and control surfaces that give highest effectiveness can be determined by theoretical studies of these flow fields. A method has been derived which predicts the trend of downwash around a circular body as the angle of attack is increased. A method has also been derived which gives good predictions of the tail contributions to lateral stability through a considerable angle-of-attack range. The method used in the lateral stability case considered the two-dimensional flow fields from the wings but not the vortex fields from the wing or the body. Further work remains to be done on longer, more slender configurations for which the vortex type of interference will probably be important.

Langley Aeronautical Laboratory,
National Advisory Committee for Aeronautics,
Langley Field, Va., November 2, 1955.

REFERENCES

1. Love, Eugene S.: Supersonic Wave Interference Affecting Stability. NACA RM L55L14a, 1956.
2. Penland, Jim A., Ridyard, Herbert W., and Fetterman, David E., Jr.: Lift, Drag, and Static Longitudinal Stability Data From an Exploratory Investigation at a Mach Number of 6.86 of an Airplane Configuration Having a Wing of Trapezoidal Plan Form. NACA RM L54L03b, 1955.
3. Ridyard, Herbert W., Fetterman, David E., Jr., and Penland, Jim A.: Static Lateral Stability Data From an Exploratory Investigation at a Mach Number of 6.86 of an Airplane Configuration Having a Wing of Trapezoidal Plan Form. NACA RM L55A21a, 1955.
4. Dunning, Robert W., and Ulmann, Edward F.: Static Longitudinal and Lateral Stability Data From an Exploratory Investigation at Mach Number 4.06 of an Airplane Configuration Having a Wing of Trapezoidal Plan Form. NACA RM L55A21, 1955.
5. Dunning, Robert W., and Ulmann, Edward F.: Exploratory Investigation at Mach Number 4.06 of an Airplane Configuration Having a Wing of Trapezoidal Plan Form - Longitudinal and Lateral Control Characteristics. NACA RM L55B28, 1955.
6. Fetterman, David E., Jr., Penland, Jim A., and Ridyard, Herbert W.: Static Longitudinal and Lateral Stability and Control Data From an Exploratory Investigation at a Mach Number of 6.86 of an Airplane Configuration Having a Wing of Trapezoidal Plan Form. NACA RM L55C04, 1955.
7. Dunning, Robert W., and Ulmann, Edward F.: Exploratory Investigation at Mach Number 4.06 of an Airplane Configuration Having a Wing of Trapezoidal Plan Form - Effects of Various Tail Arrangements on Wing-On and Wing-Off Static Longitudinal and Lateral Stability Characteristics. NACA RM L55D08, 1955.
8. Penland, Jim A., Fetterman, David E., Jr., and Ridyard, Herbert W.: Static Longitudinal and Lateral Stability and Control Characteristics of an Airplane Configuration Having a Wing of Trapezoidal Plan Form With Various Tail Airfoil Sections and Tail Arrangements at a Mach Number of 6.86. NACA RM L55F17, 1955.

SCHLIEREN FLOW PHOTOGRAPH
TOP VIEW



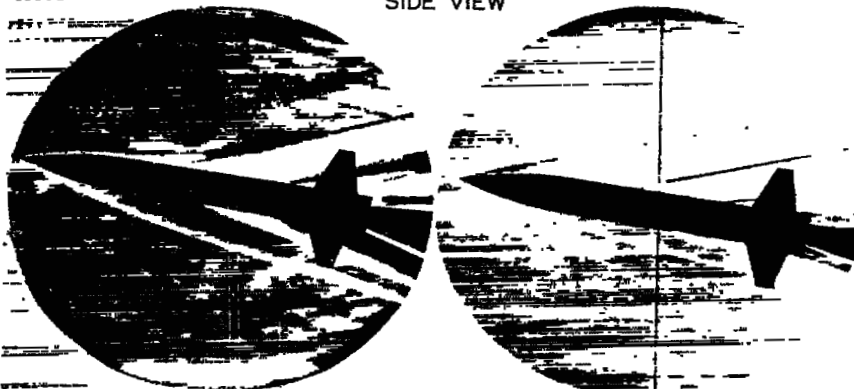
$M = 6.86$
 $\alpha = 20^\circ; \beta = 0^\circ$

Figure 1

L-91772

SCHLIEREN FLOW PHOTOGRAPHS

SIDE VIEW



$M = 4.06$
 $\alpha = 8^\circ; \beta = 0^\circ$

$M = 6.86$
 $\alpha = 8^\circ; \beta = 0^\circ$

Figure 2

L-91773

VARIATION OF DYNAMIC PRESSURE WITH MACH NUMBER
 $\alpha = 15^\circ$

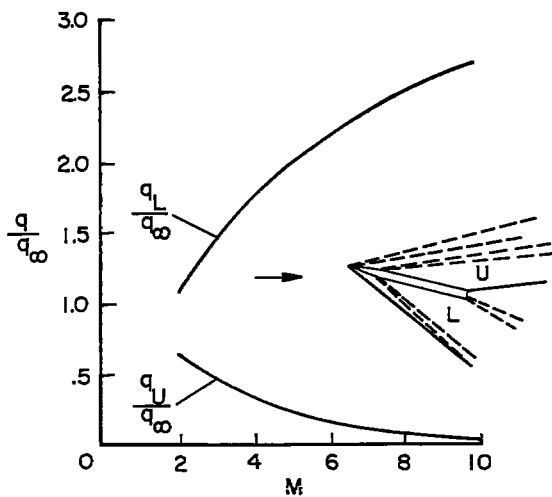


Figure 3

EFFECT OF TAIL LOCATION ON LONGITUDINAL STABILITY AND CONTROL

$M = 4, \alpha = 10^\circ$

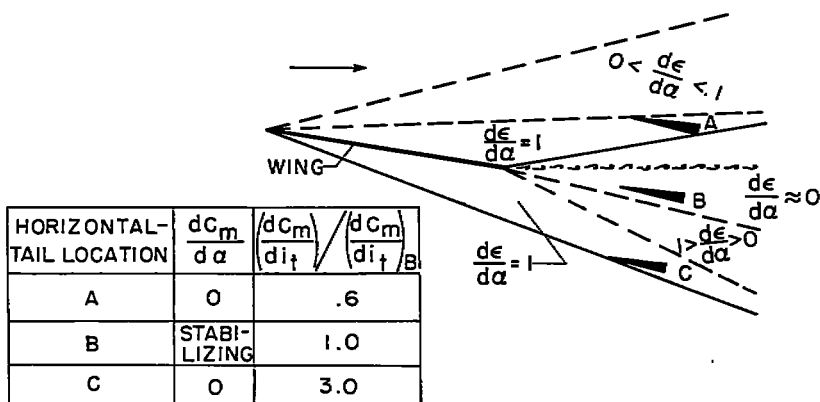


Figure 4

EFFECT OF TAIL LOCATION ON LONGITUDINAL STABILITY
 $M = 6.86$

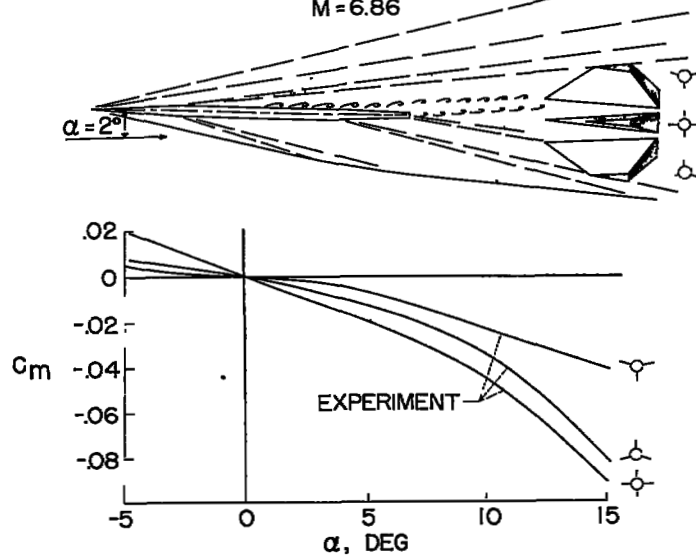


Figure 5

VARIATION OF EFFECTIVE DOWNWASH ANGLE WITH ANGLE OF
 ATTACK
 $M = 6.86$

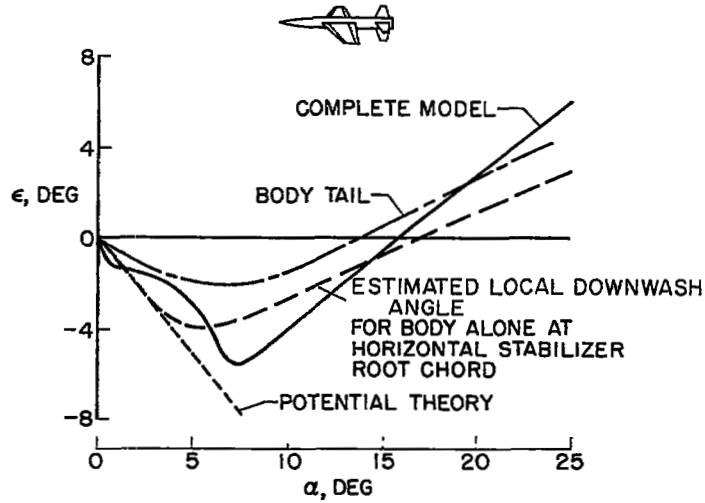


Figure 6

LONGITUDINAL STABILITY

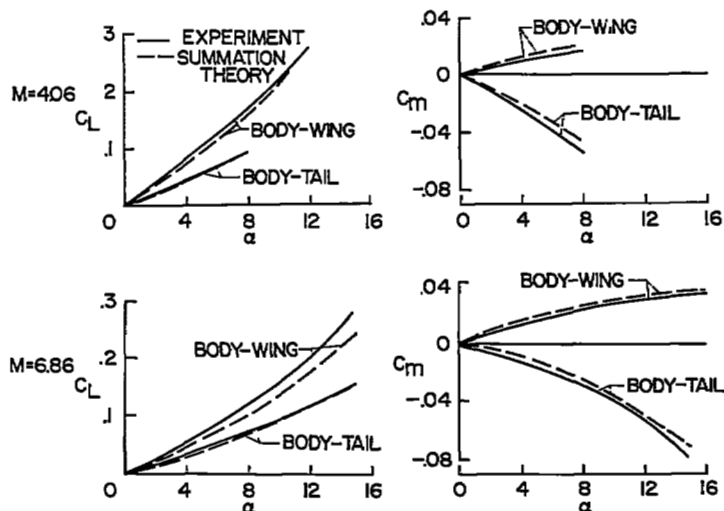


Figure 7

LONGITUDINAL STABILITY
COMPLETE MODEL

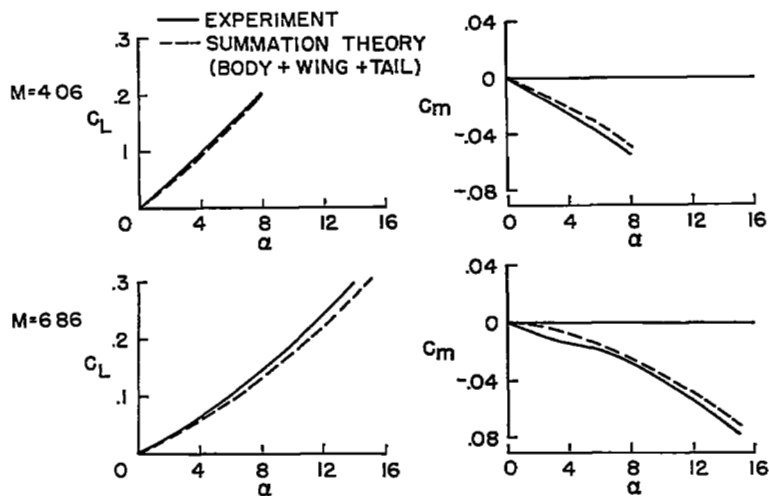


Figure 8

EFFECT OF TAIL LOCATION ON
LONGITUDINAL CONTROL

M = 6.86

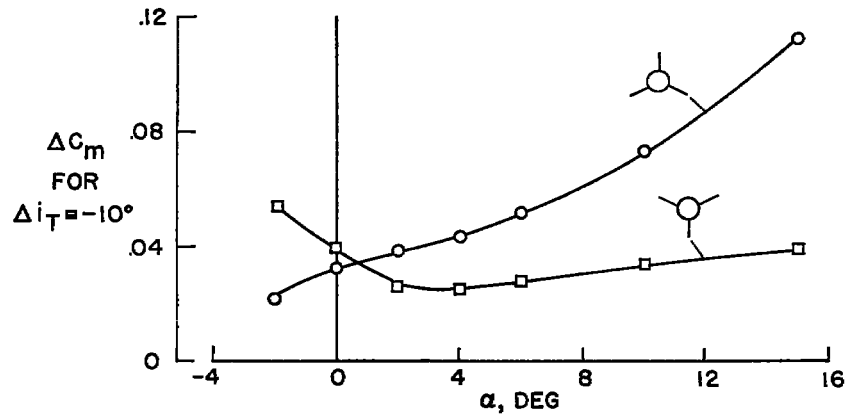


Figure 9

EFFECT OF WING ON DIRECTIONAL STABILITY

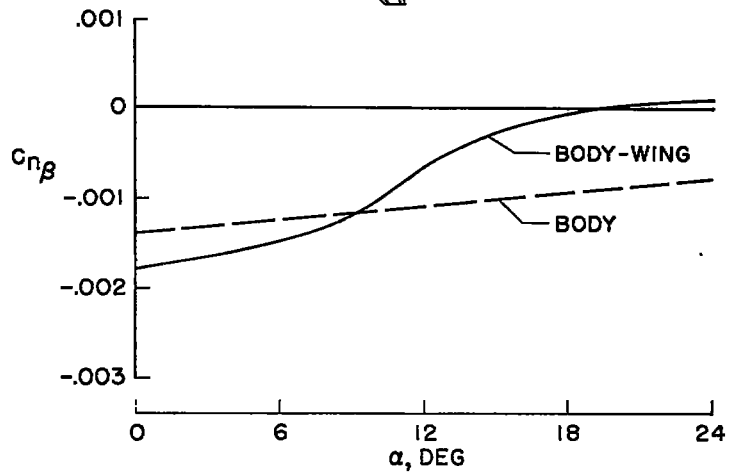


Figure 10

EFFECT OF TAIL ARRANGEMENT ON DIRECTIONAL STABILITY

M=6.86; R=343,000

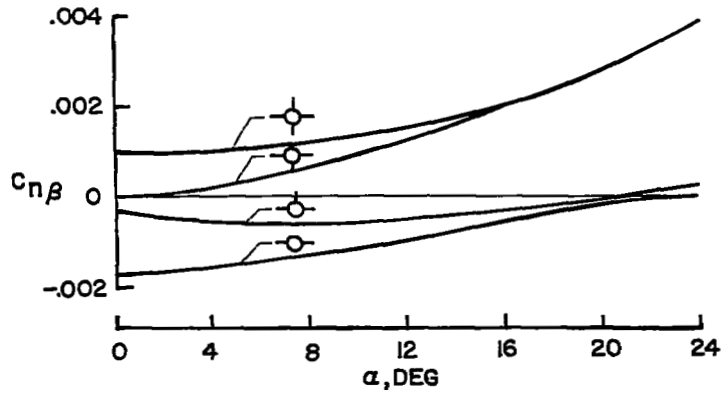


Figure 11

PREDICTION OF LATERAL STABILITY

M=4.06, R = 2.7x10⁶

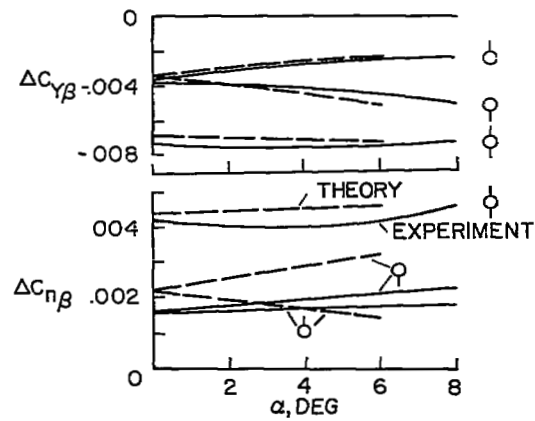
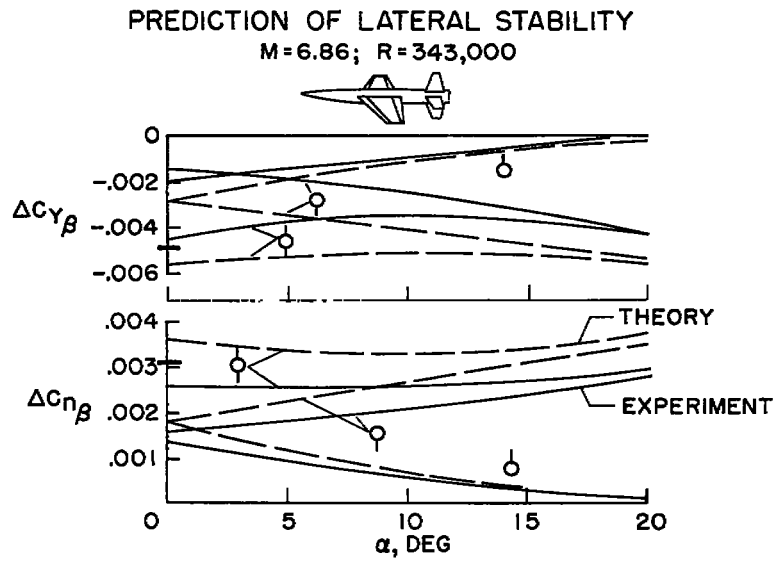


Figure 12



TEST CONFIGURATIONS
M=4.06

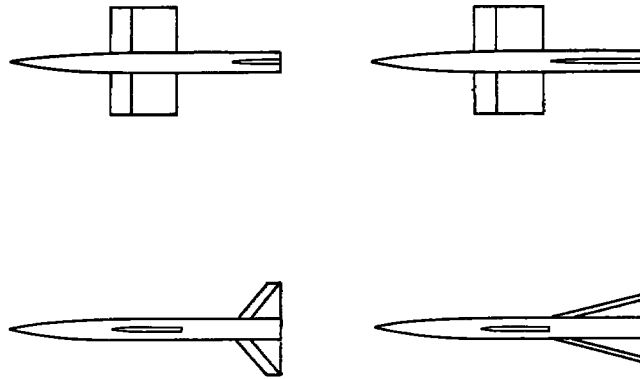


Figure 14

PREDICTION OF LATERAL STABILITY

M = 4.06 

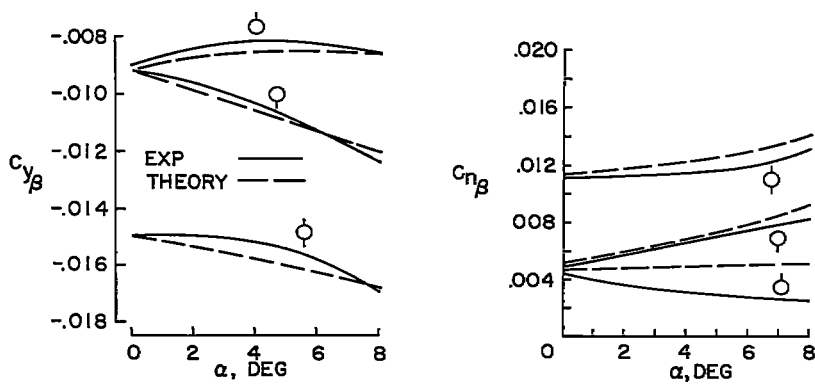


Figure 15

NASA Technical Library



3 1176 01438 0597

